Please do not adjust margins

Supporting Information

Fabrication of Sharp-edged 3D microparticles *via* folded PDMS microfluidic channels†

Received 00th January 20xx,
Accepted 00th January 20xx

DOI: 10.1039/x0xx00000x

Chenchen Zhou,[a] Shuaishuai Liang,[b] Yongjian Li,[a] Haosheng Chen,[a] and Jiang Li*[b]

Category	Tissue construct	Microgel shape	Reference
1D linear assemblies	Prism	Cuboid	1
	Tubular shape	Tubular shape	2
2D planar assemblies	Plane	Hexagonal prism; Cylinder, Triangular prism, Cube	3
	Lock-and-key shape	Rod-shaped prism Cross-shaped prism	1, 3, 4
3D spatial assemblies	Seven-layer spheroid	Cuboid	5, 6
	Multilayered 3D shape	Hexagonal prism	7

Table S1: Many investigations have been conducted to study the shapes of SEMPs and the tissue engineering application of their assemblies. SEMPs with different shapes can be assembled to form different tissue constructs, which have a significant impact on current bottom-up tissue engineering approaches.

[a.] Address here. State Key Laboratory of Tribology, Tsinghua University, Beijing 100084, China.
[b.] School of Mechanical Engineering, University of Science and Technology Beijing, Beijing 100083, China. E-mail: lijiang@ustb.edu.cn
†Electronic Supplementary Information (ESI) available. See DOI: 10.1039/x0xx00000x

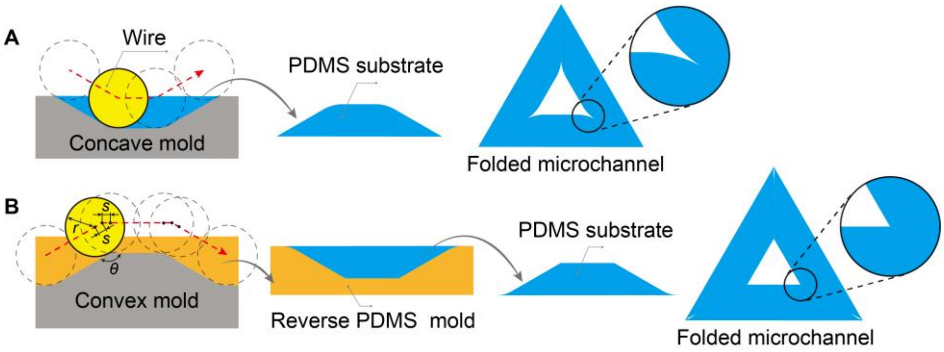

Fig. S1. Folded triangular microchannel fabrication processes based on two types of metal molds. A) Concave metal mold. After being machined by the cutting wire, the concave edges of the mold are rounded with the corner radius that equals to wire radius. The rounded features cause the wedge-shaped channel corners, which can reduce the precision of the particle features. B) Convex metal mold. Once the wire contacts the convex edges, two equal spare moving distances s ($s = r \cdot \cot(\vartheta/2)$) are added in wire's moving path. The trace of the wire is shown by the red dotted line with an arrow. The sharpness of the convex edges can be well defined, which contributes to the high precision of the folded triangular microchannel.

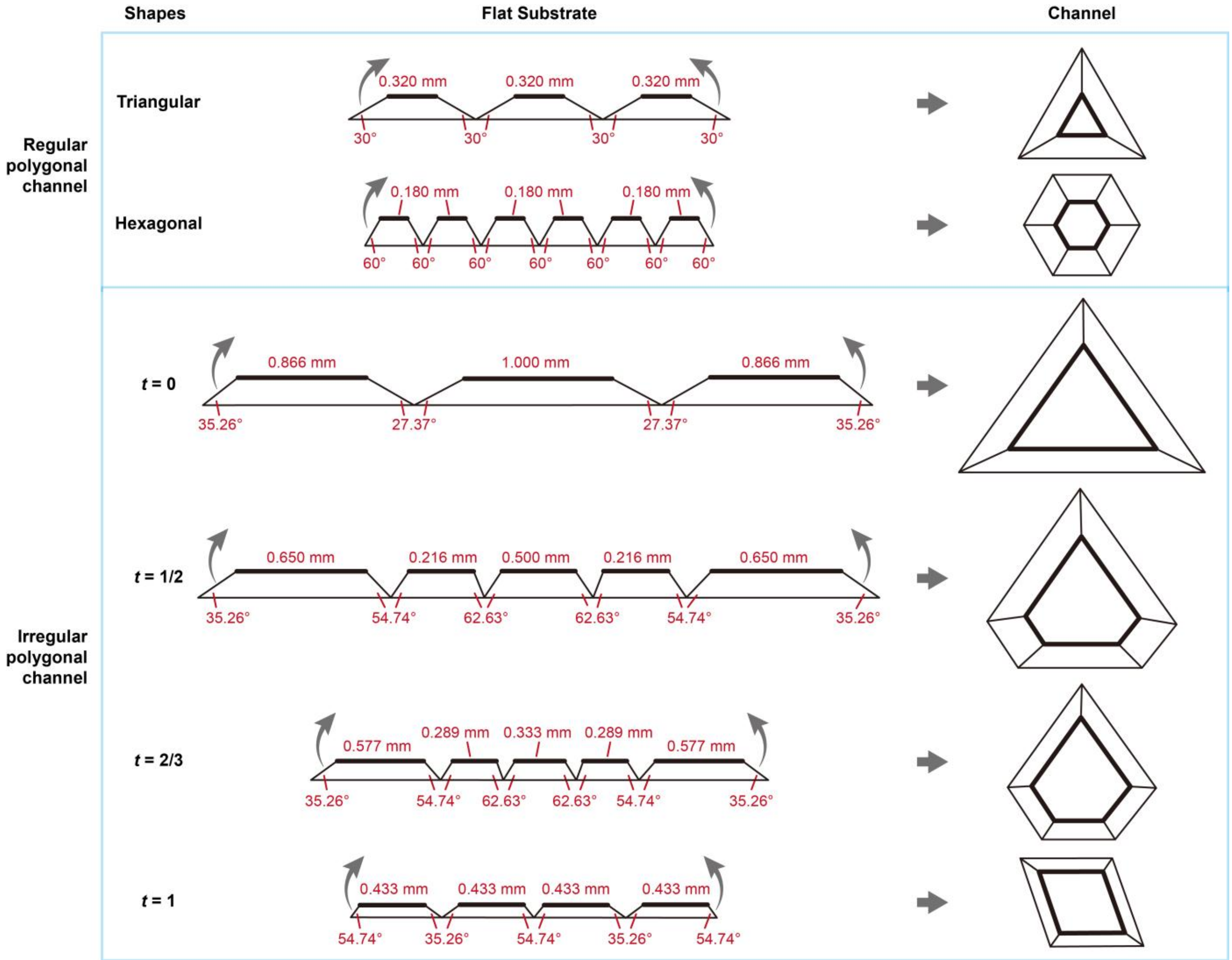

Fig. S2. The designs of the flat PDMS substrates for fabricating the regular and irregular polygonal microchannels. Convex 440C stainless steel metal molds are designed and machined according to the designs of concave PDMS molds and flat substrates. And the concave PDMS molds are then obtained by replica molding from the convex metal molds. Flat PDMS substrates are demolded from the OTS-coated PDMS molds after heating at 65°C for 45min, then they are folded into enclosed polygonal channels with PC clamps pressed on. For experimental convenience, the recommended values for the thickness h of the substrates and the length L of the channel are h = 3~6 mm and L = 20~30 mm, respectively. In our experiments, h = 5 mm, L = 25 mm for a = 1 mm.

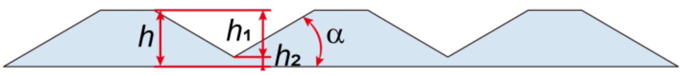

Fig. S3. The thickness of the substrate h is the thickness of the prism features (h_1) plus the thickness of the continuous connecting layer (h_2). h influences the ease with which the substrate can be folded and secured in the PC clamps. It has the appropriate range according to the slope angle of the angled surface (α): 0° < α ≤ 30°, 20μm ≤ h_2 < 40μm; 30° < α ≤ 45°, 20μm ≤ h_2 < 60μm; 45° < α ≤ 60°, 20μm ≤ h_2 < 80μm; 60° < α ≤ 75°, 20μm ≤ h_2 < 100μm; 75° < α < 90°, 20μm ≤ h_2 < 120μm.

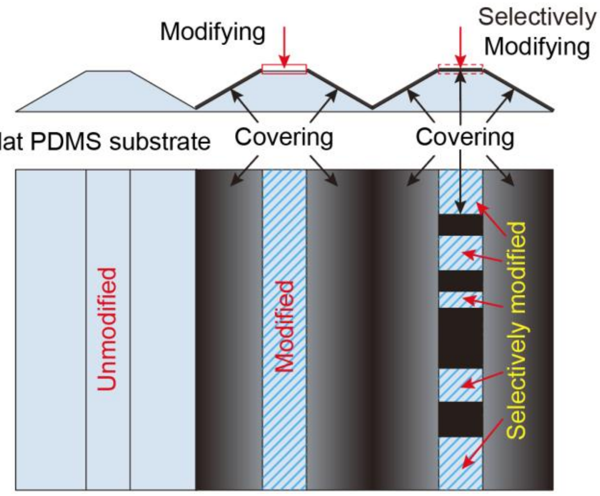

Fig. S4. Example of a procedure to selectively modify the inner walls of the microchannel. The angled surfaces of the PDMS substrate are covered during the modification process, they can still bond after removing the cover. The placement of the covers determines the modified and unmodified regions on the flat surfaces of the PDMS substrate.

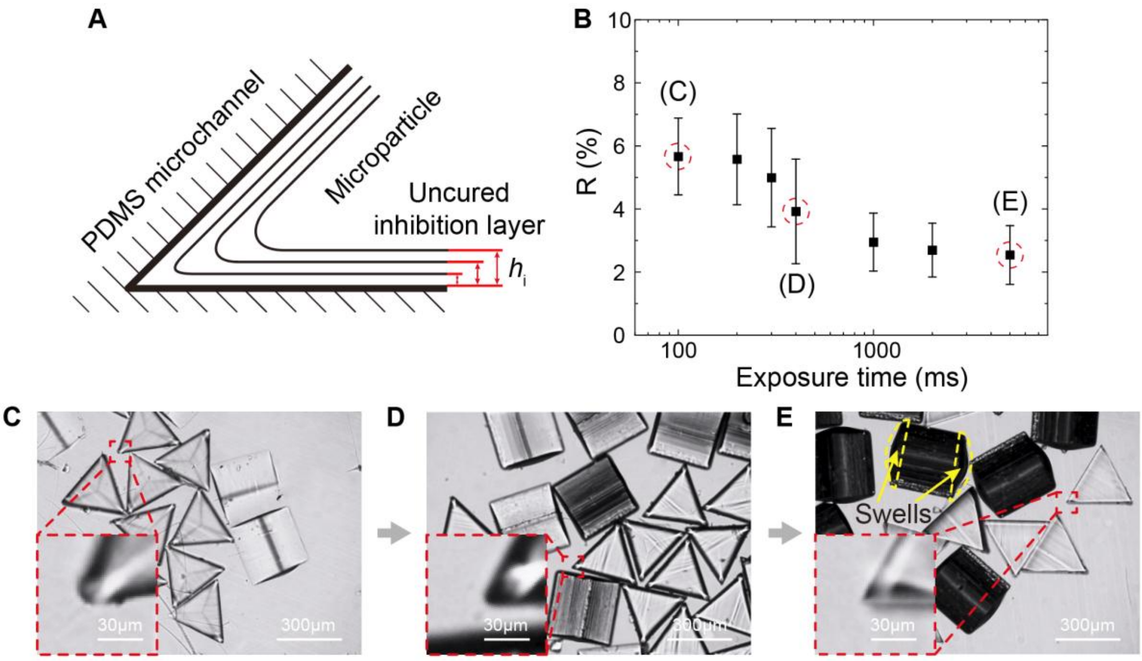

Fig. S5. Controlling the sharpness of the edge by adjusting the uncured inhibition layer in the interface between the microparticle surface and the inner wall of the PDMS microchannel. A) Schematics showing that the thinner uncured inhibition layer leads to the sharper edge. B) The relationship between the *R* and exposure time indicating that *R* decreases as the exposure time increases. C), D), E) Optical images showing the triangular microparticles fabricated with exposure time of 100ms, 400ms and 5s. The inset enlarged images showing the sharpness of the microparticle edge corner. However, the particles become out of shape when they receive too much exposure energy, there are swells at both ends of the microparticle when the exposure time is 5s.

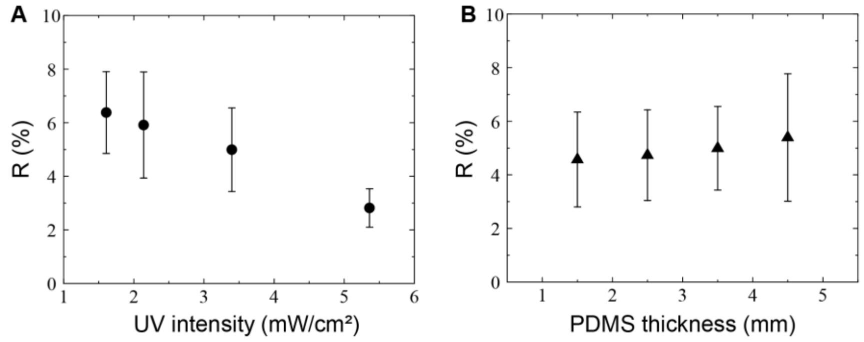

Fig. S6. Controlling the sharpness of the SMEPs edge by adjusting the UV intensity and PDMS thickness. A) The relationship between the *R* and the UV intensity indicating that *R* decreases as the UV intensity increases. B) The relationship between the *R* and PDMS thickness indicating that *R* increases slightly as the PDMS thickness increases.

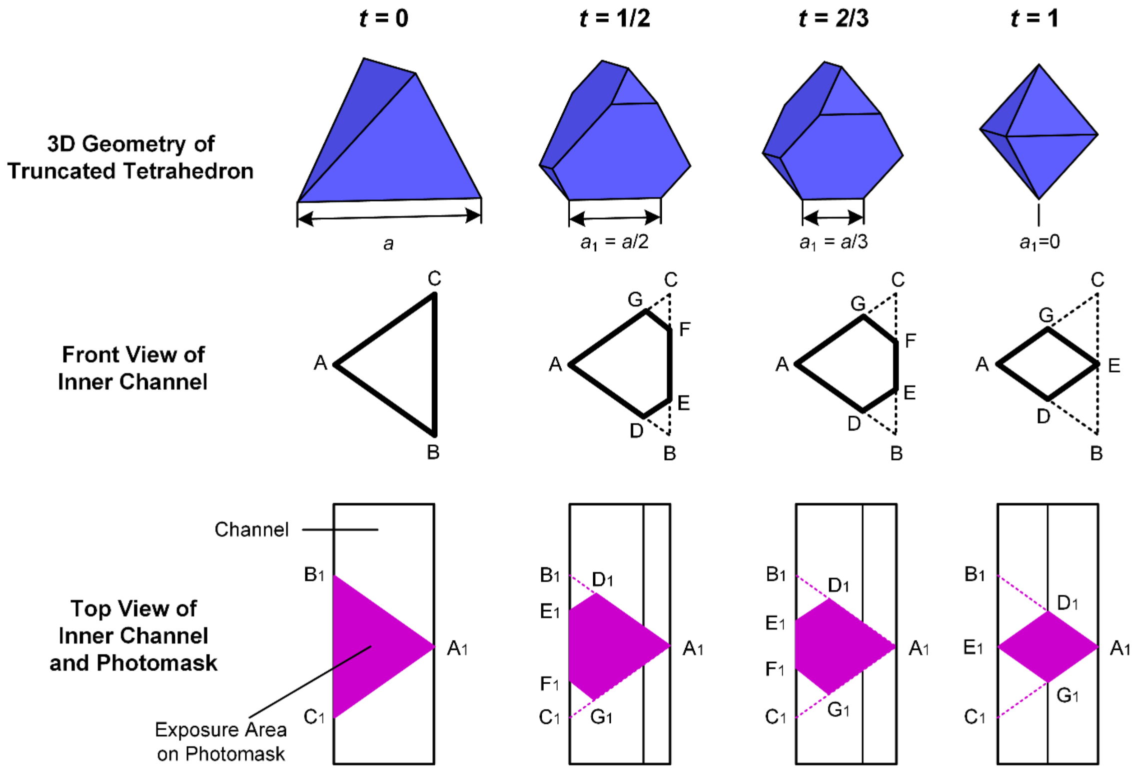

Fig. S7. The design of the polygonal channel and the photomask, and the alignment of the photomask with the polygonal channel for UV exposure. For Platonic tetrahedra with *t* = 0, a triangular channel is used. The triangular cross-section ΔABC is congruent to the triangular window $\Delta A_1B_1C_1$ on the photomask. For truncated tetrahedra with 0 < *t* < 1, a pentagonal channel is used. The pentagonal cross section ADEFG is congruent to the pentagonal window $A_1D_1E_1F_1G_1$ on the photomask. For Platonic octahedra with *t* = 1, a rhombic channel is used. The rhombic cross section ADEG is congruent to the rhombic window $A_1D_1E_1G_1$ on the photomask. There are BC = *a*, AB = AC = $\sqrt{3}a/2$, ∠BAC = 70.52°, DE // AC, GF // AB for all the cases. When *t* = 1/2, EF = a_1 = *a*/2, AD = AG = $3\sqrt{3}a/8$, DE = CG = $\sqrt{3}a/8$. When *t* = 2/3, EF = a_1 = *a*/3, AD = AG = $\sqrt{3}a/8$, DE = CG = $\sqrt{3}a/6$. When *t* = 1, AD = AG = DE = EG = $\sqrt{3}a/4$. In our experiments, *a* = 1mm; the thickness of the channel wall is *h* = 5 mm.

Particle shape	Mask shape	Channel cross-section shape	$R_{(average)}$	θ (averge)	$R_{h/b}$	$R_{l/d}$
Triangular prism	Square	Triangle	3.9%	59.1°	/	1.01
Hexagonal prism	Square	Hexagon	9.1%	121.3°	/	0.90
SEMP-A	Hexagon	Triangle	6.4%	59.6°	/	/
SEMP-B	Hexagon	Hexagon	9.5%	119.8°	/	/
SEMP-C	Triangle-rectangle-combined shape	Triangle	5.5%	58.7°	0.75	1.74
SEMP-D	Triangle-rectangle-combined shape	Hexagon	5.0%	63.1°	0.75	1.78
SEMP-E	Large circle (diameter ~310 μm)	Triangle	5.2%	60.0°	/	/
SEMP-F	Large circle (diameter ~310 μm)	Hexagon	10.7%	120.2°	/	/
SEMP-G	Medium circle (diameter ~180 μm)	Triangle	8.3%	59.8°	1.38	1.49
SEMP-H	Medium circle (diameter ~180 μm)	Hexagon	11.6%	119.5°	0.42	1.95
SEMP-I	Small circle (diameter ~120 μm)	Triangle	9.7%	59.1°	0.64	2.24
SEMP-J	Small circle (diameter ~120 μm)	Hexagon	18.3%	120.4°	0.25	2.92
Tetrahedron	Isosceles triangle	Isosceles triangle	14.4%	70.3°	/	/
Truncated tetrahedron with t = 1/2	Pentagon	Pentagon	6.7%/9.3%	70.1°/109.2°	/	/
Archimedean truncated tetrahedron with t = 2/3	Pentagon	Pentagon	9.5%/8.2%	70.7°/108.6°	/	/
Platonic octahedron with t = 1	Rhombus	Rhombus	12.4%	105.3°	/	/

Table S2. Sixteen different sharp-edged microparticles (SEMPs) we have fabricated in this work. R refers to the ratio of the edge-corner radius to the circumradius of the polygonal cross-section, θ is the average cutting angle, $R_{h/b}$ and $R_{l/d}$ are the ratio of the head to the body and the ratio of the length to diameter, respectively.

ID	Particle shape	Mask shape	Channel cross-section shape	$\theta_{(theoretical)}$
P03	Cube	Square	Square	90°
O02	Pentagonal prism	Rectangle	Pentagon	108°
O04	Heptagonal prism	Rectangle	Heptagon	128.6°
O05	Octagonal prism	Rectangle	Octagon	135°
O06	Nonagonal prism	Rectangle	Nonagon	140°
O07	Decagonal prism	Rectangle	Decagon	144°
O18	Obtuse golden rhombohedron	Rectangle	Rhombus	Obtuse angle
O19	Acute golden rhombohedron	Rectangle	Rhombus	Acute angle
O22	Square pyramid (Supercube)	Isosceles triangle	Isosceles triangle	120°
J01	Square Pyramid (Disordered)	Isosceles triangle	Isosceles triangle	/
J08	Elongated Square Pyramid	Pentagon	Pentagon	/
J15	Elongated Square Dipyramid	Pentagon	Pentagon	/
J26	Gyrobifastigium	Pentagon	Pentagon	/
J52	Augmented Pentagonal Prism	Hexagon	Pentagon	120°/108°
J54	Augmented Hexagonal Prism	Heptagon	Pentagon	120°
J55	Parabiaugmented Hexagonal Prism	Rhombus	Hexagon	/

Table S3. Sixteen different shapes listed in ref[8] can be fabricated through our method. $\theta_{(theoretical)}$ is referred to as the theoretical cutting angle.

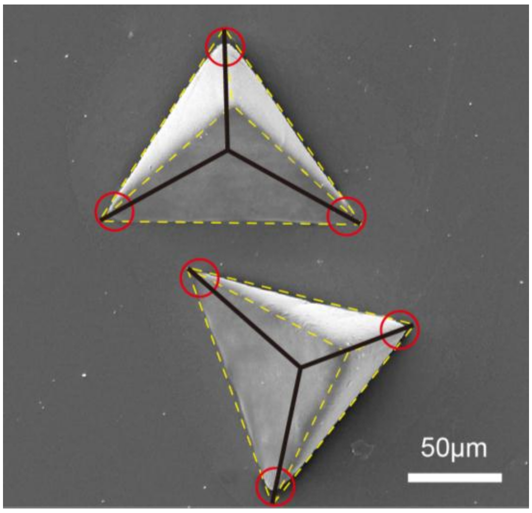

Fig. S8. The Smallest tetrahedra we have fabricated with a side length of about 120μm. The yellow dotted standard box was derived from the outline of the practical microparticles. The black continuous lines mark the top three theoretical edges of the regular tetrahedra. It can be deduced that the practical angles of the microchannel's cross-section are not precise, which is mainly responsible for the PDMS substrates alignment precision limitation. The 20μm-diameter circles were used to mark the typical sharp features on the scale < 20μm. The resolution of tetrahedral microparticles along sharp channel features on the scale ≤20μm are better than that of the microparticles fabricated through COC material[9].

Reference

1. Y. Du, E. Lo, S. Ali and A. Khademhosseini, *Proceedings of the National Academy of Sciences of the United States of America*, 2008, **105**, 9522-9527.
2. Y. Du, M. Ghodousi, H. Qi, N. Haas, W. Xiao and A. Khademhosseini, *Biotechnology and Bioengineering*, 2011, **108**, 1693-1703.
3. B. Zamanian, M. Masaeli, J. W. Nichol, M. Khabiry, M. J. Hancock, H. Bae and A. Khademhosseini, *Small*, 2010, **6**, 937-944.
4. L. Wang, M. Qiu, Q. Yang, Y. Li, G. Huang, M. Lin, T. J. Lu and F. Xu, *Acs Applied Materials & Interfaces*, 2015, **7**, 11134-11140.
5. F. Xu, T. D. Finley, M. Turkaydin, Y. Sung, U. A. Gurkan, A. S. Yavuz, R. O. Guldiken and U. Demirci, *Biomaterials*, 2011, **32**, 7847-7855.
6. Y. L. Han, Y. Yang, S. Liu, J. Wu, Y. Chen, T. J. Lu and F. Xu, *Biofabrication*, 2013, **5**.
7. F. Yanagawa, H. Kaji, Y.-H. Jang, H. Bae, Y. Du, J. Fukuda, H. Qi and A. Khademhosseini, *Journal of Biomedical Materials Research Part A*, 2011, **97A**, 93-102.
8. P. F. Damasceno, M. Engel and S. C. Glotzer, *Science*, 2012, **337**, 453-457.
9. R. Yuan, M. B. Nagarajan, J. Lee, J. Voldman, P. S. Doyle and Y. Fink, *Small*, 2018, **14**, 8.